Electronic Supplementary Information

N-Nitrosodimethylamine (NDMA) Formation and Mitigation in Potable Reuse Treatment Trains Employing Ozone and Biofiltration

FERNANDA BACARO[1,2], ERIC DICKENSON[3], REBECCA A. TRENHOLM[3], DANIEL GERRITY[1]*

[1]*Department of Civil and Environmental Engineering and Construction, University of Nevada, Las Vegas, Box 454015, 4505 S. Maryland Parkway, Las Vegas, NV 89154-4015, United States*

[2]*Trussell Technologies, Inc., 232 N. Lake Avenue Suite 300, Pasadena, CA 91101, United States*

[3]*Applied Research and Development Center, Southern Nevada Water Authority, P.O. Box 99954, Las Vegas, NV 89193, United States*

*Corresponding author. Mailing address: Department of Civil and Environmental Engineering and Construction, University of Nevada, Las Vegas, Box 454015, 4505 S. Maryland Parkway, Las Vegas, NV 89154-4015, United States. Phone: (702) 895-3955. Fax: (702) 895-3936. Email: Daniel.Gerrity@unlv.edu.

Correction: This Supplementary Information (SI) file was revised on May 20, 2024. The original version included adenosine triphosphate (ATP) data in Table S4 in units of picograms (pg). However, the ATP data had been converted to microbial equivalents (ME) using a 0.001 pg/ME conversion factor (assumes that each bacterial cell contains 2 attomoles of ATP). Therefore, the units should have been listed as ME instead of pg. This version of the SI corrects this error in Table S4.

Published in *Environmental Science: Water Research & Technology*

**Text S1.** Pilot-scale ozone-biofiltration system

The pilot-scale ozone-biofiltration system consisted of an oxygen concentrator (AirSep, Denver, CO), air dryer (Magnum 600, Ozone Solutions Inc., Hull, IA), dielectric ozone generator (Nano, Absolute Ozone, Edmonton, AB, Canada), and Venturi injector (Mazzei, Bakersfield, CA) to apply the ozone to the MBR filtrate. Twelve ozone contactors, each with a depth of 122 cm, provided a contact time of approximately 20 min, which allowed for complete ozone decay prior to biofiltration. The first four contactors were 2.5 cm in diameter, and the final eight contactors were 5 cm in diameter. Each ozone contactor had teflon tubing installed at the top for ozone off gassing, and the off gas was sent to a manganese dioxide ozone destruct system (Ozone Solutions Inc, Hull, IA).

O_3/TOC ratio, which is the applied ozone dose standardized to the total organic carbon (TOC) concentration, was used to describe the ozone dose for each experimental condition. O_3/TOC ratios were determined based on changes in UV_{254} absorbance using Eq. S1 (Gerrity et al., 2012)—an approach previously validated for the MBR filtrate (Gifford et al., 2018).

$$\Delta UV_{254} \text{ Absorbance } (\%) = 51 \times \left(\frac{O_3}{TOC}\right)^{0.63} \qquad \text{(Eq. S1)}$$

The ozonated water was collected in a small water tank (maximum residence time of ~15 min) and pumped with independent peristaltic pumps (Cole Palmer, Vernon Hills, IL) to two parallel columns, one containing anthracite (1.2 mm in diameter) and another containing biological activated carbon (BAC; 0.95 mm in diameter). The anthracite was provided by the San Jose Creek Water Reclamation Plant, in Los Angeles, CA. The BAC was exhausted GAC (Norit 820, Cabot Corporation, Alpharetta, GA) obtained from the F. Wayne Hill Water Resources Center in Gwinnet County, GA, and had previously been in use for over 10 years in the full-scale water reclamation facility. A separate column filled with the same BAC received non-ozonated MBR filtrate and served as the experimental control. All biofilter columns were 2.5 cm in diameter and packed with media to a depth of approximately 70 cm. Filter media sampling ports were located at bed depths of 7.6 cm and 42 cm. The biofilters were backwashed approximately monthly once a decrease in performance was observed. Media particles lost during the backwashing process were replaced to maintain a consistent media height of 70 cm during the study.

Figure S1. Pilot-scale ozone-biofiltration system.
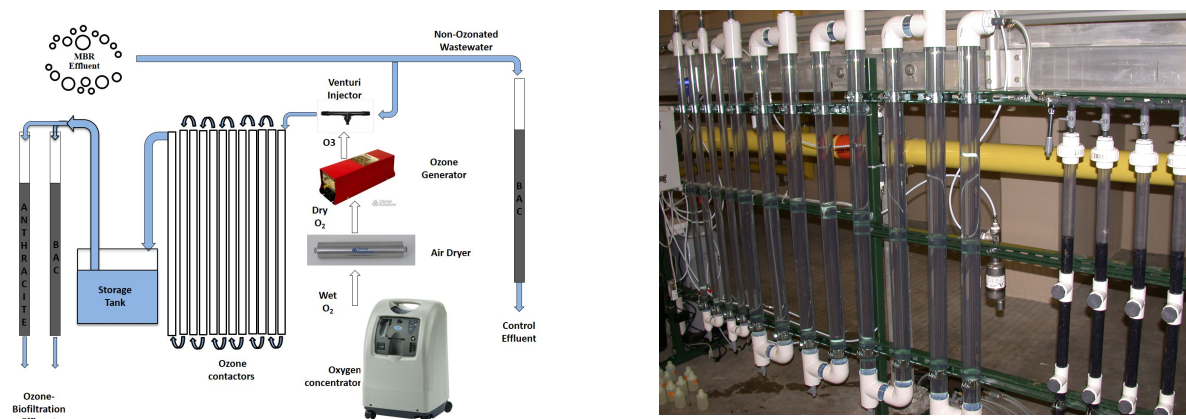
Text S2. Bulk organic matter characterization and nutrient quantification

During long-term operation of the pilot-scale system, samples were monitored weekly for TOC, UV absorbance, fluorescence, and nutrients (ammonia, nitrate, nitrite, and phosphate). TOC was measured as non-purgeable organic carbon according to Standard Method 5310B using a Shimadzu TOC-V$_{csh}$ (Kyoto, Japan). TOC samples were collected in 40-mL amber vials with Teflon-lined lids and analyzed in duplicate or triplicate (<5% relative standard deviation). All TOC samples were acidified with 400 µL of 2 N hydrochloric acid to lower the pH to <2. UV absorbance and fluorescence were quantified using an Aqualog spectrofluorometer (Horiba, Edison, NJ) after laboratory filtration with 0.7-µm glass fiber syringe filters (GD/X, Whatman, Pittsburgh, PA). For the fluorescence measurements, excitation wavelengths ranged from 240 nm to 470 nm with a 1-nm increment. Corrections for blank response, inner filter effect, and Rayleigh masking were performed within the Aqualog spectrofluorometer software. Fluorescence was also standardized to the Raman peak area of deionized water. A Matlab (MathWorks, USA) script was used to generate excitation emission matrices (EEMs) and calculate integrated regional and total fluorescence intensities (Gerrity et al., 2011). EEMs can be used to characterize dissolved organic matter and provide an estimate of soluble-microbial-product-like (region 1), fulvic-like (region 2), and humic-like (region 3) substances (Chen et al., 2003). Sample EEMs are shown in Figure S2.

Samples were also collected, diluted when necessary, and analyzed for ammonia (Hach Method 10023: salicylate method; 0.02-2.5 mg-N/L), nitrite (Hach Method 8507: diazotization method; 0.005-0.350 mg-N/L), nitrate (Hach Method 8039: cadmium reduction method; 0.3-30 mg-N/L), and phosphate (Hach Method 8048: ascorbic acid method; 0.02-2.5 mg/L as PO_4^{-3}). Ammonia, nitrate, and nitrite were measured using a DR900 multiparameter handheld colorimeter (Hach, Loveland, CO), and phosphate was measured using a DR5000 spectrophotometer (Hach).

Table S1 summarizes the effluent TOC concentrations and corresponding percent removals for the Phase 1 kinetics tests (see Section 3.1 in main text). Feed water samples were collected at the beginning and end of each test to evaluate temporal variability in feed water TOC concentration.

Table S1. Effluent TOC concentration as a function of EBCT (raw data for Figure 1).

EBCT (min)	BAC Control (No O$_3$)[1]		O$_3$-Anthracite[1]		O$_3$-BAC[1]	
	TOC (mg-C/L)	TOC Removal[2]	TOC (mg-C/L)	TOC Removal[2]	TOC (mg-C/L)	TOC Removal[2]
0 (Beginning of Test)	6.03	--	8.64	--	8.64	--
	6.80	--	8.66	--	8.66	--
0 (End of Test)	6.13	--	7.96	--	7.96	--
	6.09	--	7.94	--	7.94	--
2	5.76	8.12%	6.70	19.3%	5.96	28.2%
	5.73	8.58%	6.74	18.8%	6.24	24.9%
10	5.64	9.90%	5.35	35.6%	4.97	40.2%
	5.62	10.3%	5.37	35.4%	4.89	41.1%
20	5.62	10.3%	5.82	29.9%	5.24	36.8%
	5.47	12.7%	5.96	28.2%	5.06	39.0%

[1]Different feed waters for control vs. ozonated MBR filtrate experiments
[2]TOC removal calculated using overall average TOC at 0 minutes as the baseline

Figure S2. EEMs for (a) a typical secondary effluent (with regional delineations), (b) MBR filtrate from the current study (i.e., MBR), (c) non-ozonated BAC effluent with an EBCT of 10 minutes (i.e., MBR+BAC); (d) ozonated MBR filtrate with an O_3/TOC of 1.6 (i.e., MBR+O_3), and (e) ozonated BAC effluent with an O_3/TOC of 1.6 and EBCT of 10 minutes (i.e., MBR+O_3+BAC).
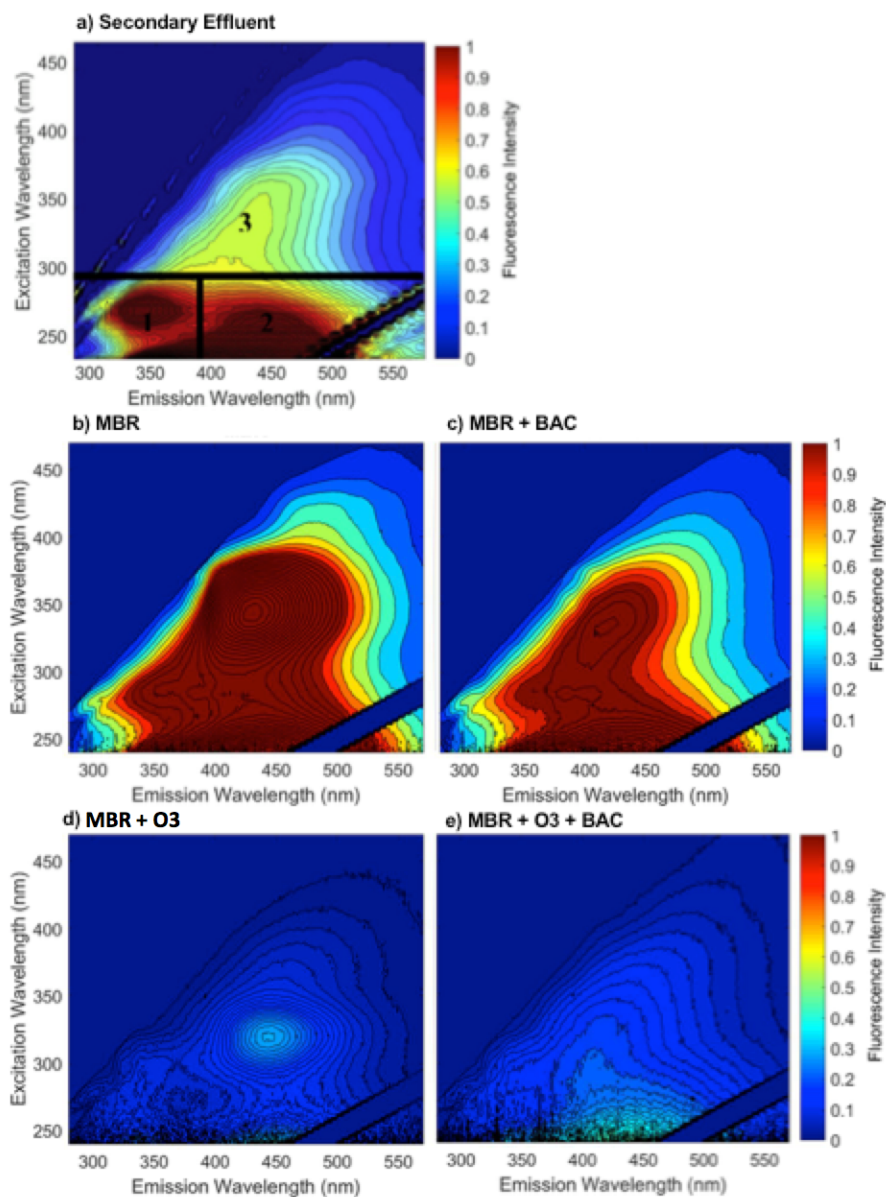
Text S3. Biodegradation of NDMA

The recent literature has identified a number of soluble methane, propane, and toluene-4 monooxygenase genes linked to NDMA biodegradation (Streger et al., 2003; Sharp et al., 2005; Sharp et al., 2007; Sharp et al., 2010; Wang et al., 2015), as summarized in Table S2.

Table S2. Bacterial strains (and the corresponding genes) known to biodegrade NDMA.

Monooxygenase Gene		Bacterial strain	Reference
soluble methane	sMMO	*Methylosinus trichosporium* OB3b	Sharp et al. 2005
propane	PrMO	*Mycobacterium vaccae* JOB5	Sharp et al. 2010
toluene 4-	T4MO	*Pseudomonas mendocina* KR1	Sharp et al. 2005
propane	PrMO	*Rhodococcus sp.* RR1	Sharp et al. 2005, 2010
toluene 4-	T4MO	*Ralstonia pickettii* PKO1*	Sharp et al. 2005
propane	PrMO	*Rhodococcus ruber* ENV 425	Streger et al. 2003
propane	PrMO	*Rhodococcus sp.* RHA1	Sharp et al. 2007
propane	PrMO	*Mycobacterium smegmatis* MC2155	Sharp et al. 2007
propane	PrMO	*Gordonia sp.* TY-5	Sharp et al. 2007
propane	PrMO	*Mycobacterium* TY-6	Sharp et al. 2010
propane	PrMO	*Pseudonocardia* TY-7	Sharp et al. 2010
propane	PrMO	*Methylibium petroleiphilum* PM1	Sharp et al. 2010
unknown		*Rhodococcus cercidiphylly* A41 AS1	Wang et al. 2015

*partial degradation

The current study targeted a subset of the genes present in the propane monooxygenase operon (PrMO) of *Rhodococcus sp.* RHA1, specifically *prm*A, *prm*B, and *prm*E (Sharp et al., 2007). These genes are also present in the genomes of other bacterial species known to biodegrade NDMA. The specific DNA sequences for the forward and reverse primers targeting *prmA* and *prmB* were found in Sharp et al. (2007). The primers targeting *prmE* were designed using the BLAST tool from the National Center for Biotechnology Information (NCBI) and the gene sequence provided by Sharp et al. (2007), which is registered in the NCBI gene database.

Figure S3. Propane monooxygenase operon in *Rhodococcus sp.* RHA1. The hatched lines indicate upregulation in the presence of propane (Sharp et al., 2007).
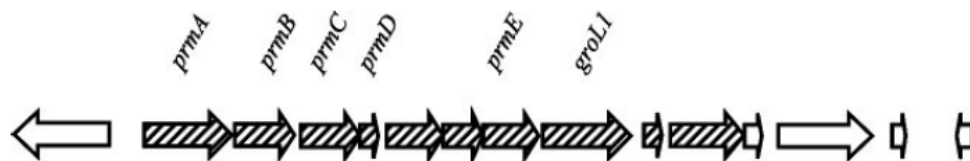
Primers were purchased from Integrated DNA Technologies (IDT, Corvalville, IA) and diluted with DNase free water (Bio-Rad, Hercules, CA) to reach a final concentration of 10 µM. Standards incorporating the primer and product sequences (total length of 129 base pairs for each gene) were also purchased from IDT and resuspended using a Tris/EDTA (TE) buffer to reach a final concentration of 10 ng/µL. The samples and standards were loaded into 96 well plates, with each well containing a total volume of 15 µL: 5.9 µL of sterile water, 7.5 µL of iTaq Universal SYBR Green Supermix (Bio-Rad, Hercules, CA), 0.3 µL of forward primer, 0.3 µL of reverse primer, and 1 µL of sample or standard.

Text S4. Comparison of media properties and attached ATP levels

As shown in Table S3, total media surface area was calculated to allow for a direct comparison between media types (Arnold et al., 2018).

Table S3. Summary of media particle characteristics.

Parameter	Units	BAC	Anthracite
Particle diameter	mm	0.95	1.20
Bulk density	g/cm^3	0.50	0.83
Particle volume	mm^3	0.45	0.90
Particle surface area	mm^2	2.83	4.52
Moisture content	%	57	33

The volume of the filter bed was calculated by multiplying the bed height by the plan area:

$V = h \times \pi \times r^2 = 70 \text{ cm} \times \pi \times (2.54 \text{ cm/2})^2 = 354.7 \text{ cm}^3 = 354{,}700 \text{ mm}^3$

Mass of BAC = Volume × Bulk Density = 354,700 mm^3 × 0.50 g/cm^3 = 177 g

Mass of Anthracite = Volume × Bulk Density = 354,700 mm^3 × 0.83 g/cm^3 = 294 g

Assuming a 64% maximum packing arrangement (i.e., a maximum volume fraction of 64% is occupied by media and the remaining is occupied by water), the total bed volume occupied by media grains can be calculated as follows:

0.64 × 354,700 mm^3 = 227,000 mm^3

The number of particles in the column can be estimated by dividing the packing volume by the volume of an individual media particle (0.45 mm^3 for BAC and 0.90 mm^3 for anthracite):

BAC: 227,000 mm^3 / 0.45 mm^3 per particle = 504,444 particles

Anthracite: 227,000 mm^3 / 0.90 mm^3 per particle = 252,222 particles

Finally, multiplying the number of particles by the particle surface area gives the total media surface area for each filter bed, as shown below. Based on this analysis, BAC filters have 25% more surface area available for biomass growth than anthracite filters. This also assumes that bacteria are unable to occupy the porous structure of BAC particles (Arnold et al., 2018).

BAC: 504,444 particles × 2.83 mm^2 per particle = 14,276 mm^2

Anthracite: 252,222 particles × 4.52 mm^2 per particle = 11,400 mm^2

% Difference: (14,276 mm^2 - 11,400 mm^2) / 11,400 mm^2 = 0.25 = 25%

Table S4. Summary of ATP loadings on media collected from each biofiltration column. ATP values were converted to "microbial equivalents" (ME) using a 0.001 picogram/ME conversion factor. This assumes that each bacterial cell contains 2 attomoles of ATP. The days indicate the duration of operation of the pilot-scale ozone-biofiltration system prior to sample collection and ATP analysis. Revised on May 20, 2024 – see note on first page of SI file.

Day	Ozonated BAC (ME/g)[a]		Ozonated Anthracite (ME/g)[a]		Non-Ozonated BAC (ME/g)[a]	
	Top[b]	Bottom[b]	Top[b]	Bottom[b]	Top[b]	Bottom[b]
7	3.25×10^8	--	2.65×10^7	--	8.88×10^8	--
14	5.98×10^8	--	7.82×10^7	--	3.39×10^9	--
34	--	8.52×10^7	--	1.65×10^8	--	4.53×10^8
55	--	4.93×10^7	--	1.13×10^8	--	1.78×10^9
60	--	4.99×10^8	--	2.55×10^8	--	2.92×10^9
101	9.94×10^8	4.97×10^8	1.46×10^8	1.26×10^8	3.75×10^9	2.69×10^9
Avg. ME/g[a]	$(6.39\pm3.36)\times10^8$	$(2.83\pm2.49)\times10^8$	$(0.84\pm0.60)\times10^8$	$(1.65\pm0.64)\times10^8$	$(26.8\pm15.6)\times10^8$	$(19.6\pm11.2)\times10^8$
Avg. ME/cm³ [c]	$(3.20\pm1.68)\times10^8$	$(1.41\pm1.25)\times10^8$	$(0.69\pm0.50)\times10^8$	$(1.37\pm0.53)\times10^8$	$(13.4\pm7.79)\times10^8$	$(9.80\pm5.60)\times10^8$
Total ATP[d]	$(7.71\pm5.74)\times10^{10}$ ME		$(3.82\pm2.11)\times10^{10}$ ME		$(40.1\pm22.3)\times10^{10}$ ME	
ATP Density[e]	$(5.40\pm4.02)\times10^6$ ME/cm²		$(3.35\pm1.85)\times10^6$ ME/cm²		$(28.1\pm15.6)\times10^6$ ME/cm²	

[a]ATP loadings based on mass of dry media (moisture content = 57% for BAC and 33% for anthracite)
[b]Top = 7.6 cm from surface and bottom = 42 cm from surface
[c]Average ATP per cm³ of bulk media (bulk density = 0.5 g/cm³ for BAC and 0.83 g/cm³ for anthracite)
[d]Based on overall ATP average and total mass of BAC (177 g) or anthracite (294 g) in each column
[e]Based on overall ATP average and total particle surface area of BAC (14,276 cm²) or anthracite (11,400 cm²)

Text S5. Summary of qPCR and 16S rRNA gene sequencing methods and data

Table S5. DNA concentrations in the biofilter media extracts.

Sample	Nanodrop (ng/µL)	Qubit (ng/µL)
Ozonated Anthracite High	14.9	15.2
Ozonated Anthracite Low	14.7	9.20
Ozonated BAC High	12.7	0.04
Ozonated BAC Low	12.2	0.04
BAC Control High	14.5	0.15
BAC Control Low	13.2	0.10

Table S6. 16S rRNA gene abundance in the biofilter media extracts.

Sample	Gene copies per gram of dry media
Ozonated Anthracite High	8.80×10^7
Ozonated Anthracite Low	2.65×10^7
Ozonated BAC High	3.06×10^4
Ozonated BAC Low	3.02×10^4
BAC Control High	3.11×10^4
BAC Control Low	3.39×10^4

For 16S rRNA gene sequencing, samples were amplified using degenerate primers targeting the V1-2 region of the 16S rRNA gene (28F and 388R; Table 1). Paired-end sequences were generated at RTLGenomics with a MiSeq sequencer (Illumina, San Diego, CA) using 2x300 bp sequencing chemistry. An 8-bp barcode was appended to each set of sequences for identification. RTLGenomics merged the forward and reverse reads using the paired-end read merger (Zhang et al., 2013) and also performed denoising and chimera checks using the UCHIME software (Edgar et al., 2011) prior to generating final mapping, multiplexed sequence, and quality files. Demultiplexing, quality score filtering, and operational taxonomic unit (OTU) assignment (97% similarity) were performed with Quantitative Insights into Microbial Ecology (QIIME 1) (v. 1.9.1; Caporaso et al., 2010), while downstream processing of raw data, including taxonomic assignments, was performed with QIIME 2 (v. 2017.6; Caporaso et al., 2017). Assignment of taxonomy was accomplished with a naïve Bayesian classifier trained on the MiDAS database (McIlroy et al., 2015), which is a manual curation of the SILVA database (release 1.23 Ref NR99) (Quast et al., 2013).

As summarized in Table S7, the Chao1 and Goods Coverage metrics indicated that sufficient sequencing depth was achieved for both anthracite samples. The upper portion of the filter bed was assigned 128 OTUs, while the lower portion of the bed was assigned 165 OTUs. Both media samples exhibited high alpha diversity based on the Shannon (anthracite high = 4.38 and anthracite low = 5.22) and Simpson indices (anthracite high = 0.88 and anthracite low = 0.95), which is consistent with typical microbial community structure in soil (Hill et al., 2003) and biofilter media (Gerrity et al., 2018). The Shannon index simultaneously accounts for OTU richness and evenness, while the Simpson index focuses on pure diversity within a sample. These values also indicate greater microbial diversity within the lower portion of the filter bed, as demonstrated previously (Gerrity et al., 2018).

Table S7. Summary of alpha diversity metrics for the anthracite biofilter media.

Alpha Diversity Metric	Anthracite High	Anthracite Low
Total Sequences	10,591	9,820
OTUs	128	165
Singles	8	11
Chao1	129	168
Shannon Index	4.38	5.22
Simpson Index	0.88	0.95
Goods Coverage	1.00	1.00

Based on taxonomic classification at the phylum level (Figure S4 and Table S8), Proteobacteria comprised the greatest relative abundance in both samples (high = 49%, low = 77%), followed by Actinobacteria (high = 39%, low = 10%), Saccharibacteria (high = 6%, low = 1%), and Chloroflexi (high = 3% and low = 5%) (Figure S4). The other 11 phyla collectively comprised 3% and 7% of the high and low samples, respectively. Similar phylum-level compositions were observed in Cydzik-Kwiatkowska and Zielinska (2016) and Li et al. (2012), who studied the microbial community structure of activated sludge and soil aquifer treatment systems, respectively.

Figure S4. Relative abundance at the phylum level for the anthracite biofilter media.
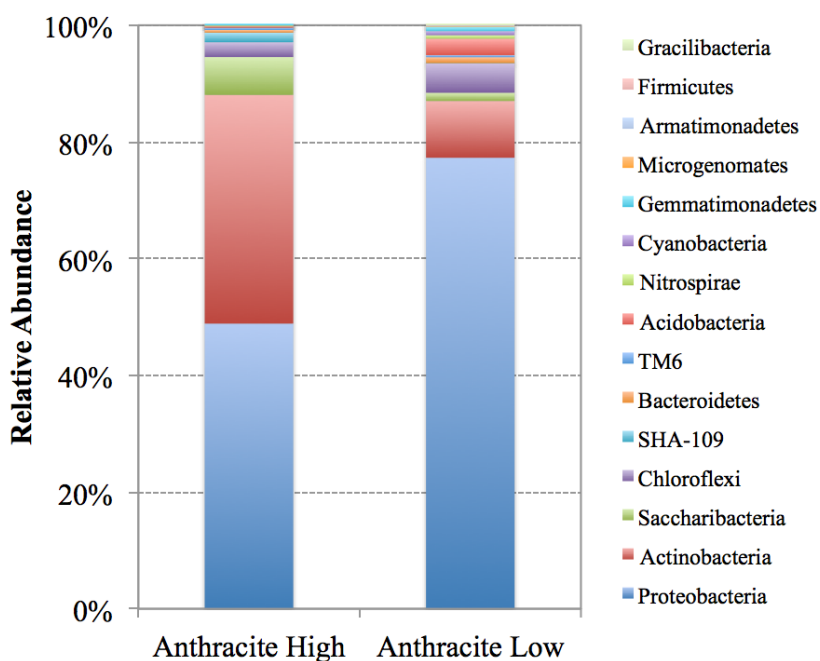
Table S8. Summary of taxonomy for the anthracite biofilter media. In the second column, the taxonomic classification refers to the genus level unless otherwise indicated (p = phylum, c = class, o = order, f = family).

Phylum	Genus	Anthracite High		Anthracite Low	
		Hits	Percent	Hits	Percent
Actinobacteria	Mycobacterium	3305	31%	788	8%
Proteobacteria	Rhodobacter	713	7%	96	1%
Saccharibacteria	Saccharibacteria[p]	683	6%	134	1%
Proteobacteria	Bradyrhizobiaceae[f]	672	6%	1264	13%
Actinobacteria	Nocardia	535	5%	73	1%
Proteobacteria	Reyranella	368	3%	755	8%
Proteobacteria	Herminiimonas	368	3%	224	2%
Proteobacteria	Hyphomicrobium	364	3%	209	2%
Proteobacteria	Afipia	303	3%	424	4%
Chloroflexi	Caldilineaceae[f]	233	2%	460	5%
Proteobacteria	Meganemaceae[f]	231	2%	188	2%
Proteobacteria	Shinella	221	2%	136	1%
Proteobacteria	Pedomicrobium	197	2%	242	2%
SHA-109	SHA-109[p]	175	2%	5	0%
Proteobacteria	Bosea	149	1%	104	1%
Actinobacteria	Pseudonocardia	142	1%	15	0%
Proteobacteria	Hydrogenophaga	133	1%	496	5%
Proteobacteria	Phyllobacteriaceae[f]	121	1%	70	1%
Proteobacteria	Nordellaceae[f]	109	1%	96	1%
Proteobacteria	Mesorhizobium	94	1%	69	1%
Proteobacteria	Caulobacteraceae[f]	81	1%	1074	11%
Proteobacteria	Rhizobiales[o]	80	1%	83	1%
Proteobacteria	Alphaproteobacteria[c]	77	1%	10	0%
Proteobacteria	Acidovorax	74	1%	140	1%
Proteobacteria	Methylorosula	69	1%	54	1%
Proteobacteria	Bradyrhizobiaceae[f]	52	0%	165	2%
Actinobacteria	Corynebaceriales[o]	49	0%	8	0%
Proteobacteria	Devosia	47	0%	40	0%
TM6	TM6[p]	42	0%	33	0%
Proteobacteria	Variibacter	41	0%	60	1%
Bacteroidetes	Chitinphagaceae[f]	39	0%	16	0%
Proteobacteria	Comamonadaceae[f]	37	0%	144	1%
Proteobacteria	Rhizobiaceae[f]	33	0%	9	0%
Proteobacteria	Hyphomicrobiaceae[f]	31	0%	48	0%
Proteobacteria	Nordella	30	0%	39	0%

Phylum	Genus	Anthracite High		Anthracite Low	
		Hits	Percent	Hits	Percent
Actinobacteria	Actinobacteria[c]	29	0%	0	0%
Proteobacteria	Aminobacter	28	0%	17	0%
Proteobacteria	MNG7	27	0%	51	1%
Actinobacteria	Lysinimonas	27	0%	9	0%
Chloroflexi	JG30-KF-CM45[o]	26	0%	4	0%
Proteobacteria	Nitrosomonadaceae[f]	22	0%	114	1%
Proteobacteria	Oxalobacteraceae[f]	22	0%	11	0%
Proteobacteria	Rhodoplanes	21	0%	114	1%
Proteobacteria	Brevundimonas	21	0%	35	0%
Proteobacteria	TRA3-20[o]	20	0%	102	1%
Proteobacteria	Phreatobacter	17	0%	1	0%
Acidobacteria	Subgroup 6[o]	16	0%	139	1%
Nitrospirae	Nitrospira	16	0%	60	1%
Proteobacteria	Cand. Alysiosphaera	16	0%	30	0%
Proteobacteria	Sphingopyxis	16	0%	10	0%
Proteobacteria	AKYH478[f]	14	0%	24	0%
Actinobacteria	Fodinicola	14	0%	2	0%
Proteobacteria	Roseomonas	13	0%	204	2%
Proteobacteria	Methylibium	12	0%	36	0%
Proteobacteria	Simplicispira	12	0%	26	0%
Proteobacteria	Defluvimonas	11	0%	8	0%
Proteobacteria	Rhodopseudomonas	11	0%	6	0%
Proteobacteria	Phyllobacteriaceae[f]	11	0%	0	0%
Proteobacteria	Nitrosomonas	10	0%	55	1%
Proteobacteria	Acidibacter	9	0%	39	0%
Proteobacteria	Rhizobacter	9	0%	15	0%
Proteobacteria	Coxiella	9	0%	8	0%
Proteobacteria	Nitratireductor	9	0%	7	0%
Actinobacteria	Microbacteriaceae[f]	9	0%	1	0%
Proteobacteria	Bauldia	8	0%	17	0%
Proteobacteria	Rhodospirillaceae[f]	7	0%	21	0%
Proteobacteria	Bradyrhizobium	7	0%	19	0%
Proteobacteria	JG35-K1-AG5	7	0%	15	0%
Chloroflexi	TK10[c]	7	0%	11	0%
Proteobacteria	Sphingomonadaceae[f]	7	0%	11	0%
Actinobacteria	LF_BF07	7	0%	5	0%
Actinobacteria	Nocardiaceae[f]	7	0%	3	0%
Acidobacteria	p7o14	6	0%	113	1%

Phylum	Genus	Anthracite High		Anthracite Low	
		Hits	Percent	Hits	Percent
Proteobacteria	Pseudomonas	6	0%	22	0%
Proteobacteria	Starkeya	6	0%	12	0%
Proteobacteria	Alphal Cluster[f]	6	0%	12	0%
Proteobacteria	Achromobacter	6	0%	2	0%
Proteobacteria	Rhizomicrobium	5	0%	17	0%
Proteobacteria	D05-2[f]	5	0%	8	0%
Actinobacteria	Tsukamurella	5	0%	0	0%
Cyanobacteria	Obscuribacterales[o]	4	0%	51	1%
Proteobacteria	Caulobacter	4	0%	27	0%
Proteobacteria	Phenylobacterium	4	0%	15	0%
Bacteroidetes	Cytophagaceae[f]	4	0%	12	0%
Proteobacteria	Rhizobium	4	0%	5	0%
Saccharibacteria	Saccharibacteria[p]	4	0%	5	0%
Proteobacteria	Hyphomicrobiaceae[f]	4	0%	5	0%
Proteobacteria	Aquamicrobium	4	0%	1	0%
Actinobacteria	Nocardioidaceae[f]	4	0%	0	0%
Proteobacteria	DB1-14[o]	4	0%	0	0%
Proteobacteria	Rhodobacteraceae[f]	4	0%	0	0%
Actinobacteria	ML817J-10	3	0%	24	0%
Actinobacteria	Iamia	3	0%	11	0%
Proteobacteria	Comamonadaceae[f]	3	0%	5	0%
Proteobacteria	Comamonas	3	0%	5	0%
Actinobacteria	Williamsia	3	0%	1	0%
Proteobacteria	Xanthobacter	3	0%	0	0%
Gemmatimonadetes	Gemmatimonas	2	0%	36	0%
Proteobacteria	Caulobacteraceae[f]	2	0%	16	0%
Proteobacteria	A0839[f]	2	0%	15	0%
Actinobacteria	Microthricaceae[f]	2	0%	11	0%
Proteobacteria	Inquilinus	2	0%	10	0%
Proteobacteria	MNC12[f]	2	0%	8	0%
Proteobacteria	Pseudolabrys	2	0%	6	0%
Proteobacteria	Gammaproteobacteria[c]	2	0%	5	0%
Proteobacteria	Woodsholea	2	0%	5	0%
Proteobacteria	Aquicella	2	0%	4	0%
Proteobacteria	Blastomonas	2	0%	4	0%
Bacteroidetes	Haliscomenobacter	2	0%	3	0%
Chloroflexi	Anaerolineaceae[f]	2	0%	3	0%
Actinobacteria	480-2[f]	2	0%	2	0%

Phylum	Genus	Anthracite High		Anthracite Low	
		Hits	Percent	Hits	Percent
Proteobacteria	Hyphomonas	2	0%	2	0%
Proteobacteria	Xanthomonadaceae[f]	2	0%	2	0%
Actinobacteria	Acidimicrobiales[o]	2	0%	1	0%
Bacteroidetes	Chryseolinea	2	0%	1	0%
Actinobacteria	S18	2	0%	1	0%
Proteobacteria	Acidiferrobacter	2	0%	0	0%
Proteobacteria	Legionella	2	0%	0	0%
Proteobacteria	Proteobacteria[p]	2	0%	0	0%
Proteobacteria	Betaproteobacteria[c]	1	0%	7	0%
Proteobacteria	Burkholderiales[o]	1	0%	5	0%
Proteobacteria	Xanthobacteraceae[f]	1	0%	5	0%
Proteobacteria	Rhodospirillaceae[f]	1	0%	5	0%
Acidobacteria	mb2424[f]	1	0%	3	0%
Proteobacteria	Rhodobiaceae[f]	1	0%	2	0%
Chloroflexi	Roseiflexaceae[f]	1	0%	1	0%
Proteobacteria	Beijerinckiaceae[f]	1	0%	1	0%
Bacteroidetes	Lewinella	0	0%	55	1%
Gemmatimonadetes	C1711WL	0	0%	21	0%
Proteobacteria	Parvularcula	0	0%	17	0%
Gemmatimonadetes	Gemmatimonadaceae[f]	0	0%	14	0%
Proteobacteria	Acidocella	0	0%	12	0%
Proteobacteria	Meganema	0	0%	11	0%
Acidobacteria	Subgroup 6[o]	0	0%	11	0%
Proteobacteria	Cupriavidus	0	0%	10	0%
Microgenomates	Microgenomates[p]	0	0%	10	0%
Proteobacteria	Hirschia	0	0%	9	0%
Cyanobacteria	Obscuribacteraceae[f]	0	0%	9	0%
Proteobacteria	KCM-B-15[f]	0	0%	9	0%
Armatimonadetes	Armatimonadales[o]	0	0%	8	0%
Chloroflexi	mle1-48	0	0%	8	0%
Proteobacteria	Acetobacteraceae[f]	0	0%	8	0%
Bacteroidetes	PHOS-HE28	0	0%	7	0%
Acidobacteria	Acidobacteria[c]	0	0%	5	0%
Firmicutes	Bacillus	0	0%	5	0%
Cyanobacteria	Vampirovibrionales[o]	0	0%	5	0%
Proteobacteria	Byssovorax	0	0%	4	0%
Bacteroidetes	Saprospiraceae[f]	0	0%	4	0%
Gemmatimonadetes	Gemmatimonadaceae[f]	0	0%	4	0%

Phylum	Genus	Anthracite High		Anthracite Low	
		Hits	Percent	Hits	Percent
Proteobacteria	Dokdonella	0	0%	3	0%
Proteobacteria	Lautropia	0	0%	3	0%
Proteobacteria	Steroidobacteraceae[f]	0	0%	3	0%
Proteobacteria	Tepidicella	0	0%	3	0%
Bacteroidetes	AKYH767[f]	0	0%	3	0%
Chloroflexi	KD4-96[c]	0	0%	3	0%
Proteobacteria	B79[f]	0	0%	3	0%
Proteobacteria	I-10[f]	0	0%	3	0%
Proteobacteria	Arenimonas	0	0%	2	0%
Proteobacteria	GR-WP33-30[o]	0	0%	2	0%
Acidobacteria	mb2424[f]	0	0%	2	0%
Proteobacteria	Nannocystis	0	0%	2	0%
Proteobacteria	NKB5[o]	0	0%	2	0%
Acidobacteria	PAUC26f[f]	0	0%	2	0%
Acidobacteria	SBRFL126	0	0%	2	0%
Proteobacteria	SC-I-84[o]	0	0%	2	0%
Proteobacteria	Tahibacter	0	0%	2	0%
Proteobacteria	Xanthomonadales[o]	0	0%	2	0%
Chloroflexi	mle1-48[f]	0	0%	2	0%
Cyanobacteria	Cand. Obscuribacter	0	0%	2	0%
Gracilibacteria	Gracilibacteria[p]	0	0%	2	0%
Proteobacteria	Asticcacaulis	0	0%	2	0%
Proteobacteria	DA111[f]	0	0%	2	0%
Acidobacteria	Bryobacter	0	0%	1	0%
Proteobacteria	Steroidobacter	0	0%	1	0%

Text S6. References

Arnold, M.A., Batista, J.R., Dickenson, E., & Gerrity, D. (2018) Use of Ozone-Biofiltration for Bulk Organic Removal and Disinfection Byproduct Mitigation in Potable Reuse Applications. Chemosphere 202, 228-237.

Caporaso, J.G., Kuczynski, J., Stombaugh, J., Bittinger, K., Bushman, F.D., Costello, E.K., Fierer, N., Pena, A.G., Goodrich, J.K., Gordon, J.I., Huttley, G.A., Kelley, S.T., Knights, D., Koenig, J.E., Ley, R.E., Lozupone, C.A., McDonald, D., Muegge, B.D., Pirrung, M., Reeder, J., Sevinsky, J.R., Turnbaugh, P.J., Walters, W.A., Widmann, J., Yatsunenko, T., Zaneveld, J., Knight, R. (2010). QIIME allows analysis of high-throughput community sequencing data. Nature Methods 7(5), 335-336.

Caporaso, J.G. (2017). Quantitative Insights into Microbial Ecology (QIIME) 2. https://qiime2.org. Accessed: Aug. 28, 2018.

Cydzik-Kwiatkowska, A., Zielinska, M. (2016). Bacterial communities in full-scale wastewater treatment systems. World J. Microbiol. Biotechnol. 32(4), 66.

Edgar, R.C., Haas, B.J., Clemente, J.C., Quince, C., Knight, R. (2011). UCHIME improves sensitivity and speed of chimera detection. Oxford J. Bioinformatics 27(16), 2194-2200.

Gerrity, D., Gamage, S., Holady, J.C., Mawhinney, D.B., Quiñones, O., Trenholm, R.A., Snyder, S.A. (2011). Pilot-scale evaluation of ozone and biological activated carbon for trace organic contaminant mitigation and disinfection. Water Res. 45(5), 2155-2165.

Gerrity, D., Gamage, S., Jones, D., Korshin, G.V., Lee, Y., Pisarenko, A., Trenholm, R.A., von Gunten, U., Wert, E.C., Snyder, S.A. (2012). Development of surrogate correlation models to predict trace organic contaminant oxidation and microbial inactivation during ozonation. Water Res. 46(19), 6257-6272.

Gifford, M., Selvy, A., Gerrity, D. (2018). Optimizing ozone-biofiltration systems for organic carbon removal in potable reuse applications. Ozone Sci. Eng. In press.

Hill, T.C.J., Walsh, K.A., Harris, J.A., Moffett, B.F. (2003). Using ecological diversity measures with bacterial communities. FEMS Microbiol Ecol. 43, 1-11.

Li, D., Sharp, J.O., Saikaly, P.E., Alidina, M., Alawari, M.S., Keller, S., Hoppe-Jones, C., Drewes, J. (2012). Dissolved organic carbon influences microbial community composition and diversity in managed aquifer recharge systems. Appl. Environ. Microbiol. 78(19), 6819 - 6828.

McIlroy, S.J., Saunders, A.M., Albertsen, M., Nierychlo, M., McIlroy, B., Hansen, A.A., Karst, S.M., Nielsen, J.L., Nielsen, P.H. (2015). MiDAS: The field guide to the microbes of activated sludge. Database. bav062.

Quast, C., Pruesse, E., Yilmaz, P., Gerken, J., Schweer, T., Yarza, P., Peplies, J., Glockner, F.O. (2013). The SILVA ribosomal RNA gene database project: Improved data processing and web-based tools. Nucleic Acids Res. 41, D590-D596.

Sharp, J. O., Sales, C. M., Alvarez-Cohen, L. (2010). Functional characterization of propane-enhanced N-nitrosodimethylamine degradation by two actinomycetales. Biotechnol. Bioeng. 107(6), 924-932.

Sharp, J.O., Sales, C.M., LeBlanc, J.C., Liu, J., Wood, T.K., Eltis, L.D., Mohn, W.W., Alvarez-Cohen, L. (2007). An inducible propane monooxygenase is responsible for N-nitrosodimethylamine degradation by *Rhodococcus sp.* strain RHA1. Appl. Environ. Microbiol. 73(21), 6930-6938.

Sharp, J.O., Wood, T.K., Alvarez-Cohen, L. (2005). Aerobic biodegradation of *N*-nitrosodimethylamine (NDMA) by axenic bacterial strains. Biotechnol. Bioeng. 89(5), 608-618.

Streger, S.H., McClay, K., Condee, C., Schuster, R., Steffan, R.J., Hatzinger, P.B. (2003). Evaluation of bioremediation options for the treatment of groundwater contaminated with *N*-nitrosodimethylamine. 103rd General Meeting of the American Society for Microbiology. Washington, D.C.

Wang, W., Guo, Y., Yang, Q., Huang, Y., Zhu, C., Fan, J., Pan, F. (2015). Characterization of the microbial community structure and nitrosamine-reducing isolates in drinking water biofilters. Sci. Tot. Environ. 521-522, 219-225.

Zhang, J., Kobert, K., Flouri, T., Stamatakis, A. (2013). PEAR: A fast and accurate Illumina Paired-End reAd mergeR. Bioinformatics 30(5), 614-620.